# High Selective Balanced Bandpass Filters Using End-Connected Conductor-Backed Coplanar Waveguide

## JIAN-KANG XIAO [1], XING QI[1], HUI-XIA WANG[1], AND JIAN-GUO MA[2], (Fellow, IEEE)

[1]School of Electro-Mechanical Engineering, Xidian University, Xi'an 710071, China
[2]School of Computers, Guangdong University of Technology, Guangzhou 510006, China

Corresponding author: Jian-Guo Ma (majg@gdut.edu.cn)

**ABSTRACT** In this paper, an end-connected conductor-backed coplanar waveguide (CBCPW) balanced bandpass filter and a size reduction one with adjustable multiple transmission zeros have been developed by using the separated electric and magnetic coupling, and quarter-wavelength short-circuited stubs. The differential mode (DM) and the common mode (CM) equivalent transmission line circuits have been modeled and verified, and the DM/CM parts can be designed individually. The proposed CBCPW balanced bandpass filters have been fabricated and measured, and their advantages of multiple transmission zeros, high out-of-band suppression, and high common mode suppression characteristics have been demonstrated.

**INDEX TERMS** Conductor-backed coplanar waveguide, balanced bandpass filter, separated electric and magnetic coupling, transmission zeros.

## I. INTRODUCTION

With the rapid development of wireless communication systems and technologies, balanced circuits have been paid more and more attention because of their superior advantages of high degree of immunity to environmental noise and lower electromagnetic interference compared with the classical single-ended devices. Many methods have been used to implement the balanced bandpass filters (BPFs) [1]–[11]. In [1] and [2], λ/4 open-circuited stubs were used to design balanced BPFs. The advantage of the design was its enhanced filter bandwidth by increasing the order of the branch lines, however, the selectivity of the DM passband was limited. In order to improve the selectivity of DM response, λ/4 stubs had been replaced by 3λ/4 stubs in [3] and [4], and transmission zeros had been realized. In [5], parallel coupled lines were utilized in balanced BPF design for achieving the desired CM suppression by placing short-circuited self-coupled ring resonator between the differential lines, while the DM passband kept independent. In [6], balanced BPFs with simple T-shaped structures were proposed, while in [7] and [8], balanced BPFs with dual-mode and multi-mode resonators had been implemented, respectively. In [9], a balanced bandpass filter with mixed electric and magnetic

coupling by using parallel coupled lines was proposed, while in [10], open-loop magnetically coupled resonators were used to design balanced bandpass filters. The frequency selectivity of both designs had been enhanced by electromagnetic coupling, however, for a pair of transmission zeros (TZs) in DM responses, more resonators would be desired, which would bring an increased circuit dimensions.

CBCPW has advantages of facilitating easy shunt and series surface mounting without requiring via holes, less electromagnetic waves leakage which brings better electromagnetic compatibility characteristic because of the co-plane of the conductor strip and the ground. Moreover, power capability can be enhanced due to the conductor-backed ground compared to the traditional coplanar waveguide (CPW). It has been noted from the references that most of the reported microwave filters are microstrip structures, few CPW/CBCPW works have been implemented.

In this paper, high selective balanced bandpass filters with multiple transmission zeros by using end-connected conductor-backed coplanar waveguide have been presented for the first time. The equivalent transmission line circuits of the balanced BPFs have been modeled and analyzed, and have been verified by calculation/simulation. Filter TZs

are attributed to the SEMC, source-load coupling, and the quarter-wavelength short-circuited stubs in differential mode (DM). TZs can be controlled/adjusted by electromagnetic couplings, and the length of the stubs. The quarter-wavelength open-circuited stubs have been used to achieve common mode (CM) rejection. Having the proper electric, magnetic couplings and the quarter-wavelength stubs, the proposed balanced BPFs can provide good common mode noise suppression but keeping the in-band responses of the differential mode unimportant changing, while the out-band responses have only small alteration, which indicates that the common mode rejection is independent of the differential mode design, so the design process can be simplified significantly. CBCPW structure is more easy for fabrication because via holes are not needed. It is also noticed in the research that end-connected CBCPW structure has less electromagnetic leakage than the CBCPW structure, which in turn enhances the electromagnetic couplings. The balanced BPFs have been fabricated, and the designs have been demonstrated by measurements.

This paper is organized as follows. Firstly, parallel-coupled line circuits of the balanced BPF are modeled, and the differential mode and the common mode are analyzed. Secondly, the proposed balanced BPF is implemented by the end-connected CBCPW, while the TZs in DM responses and the electromagnetic couplings are analyzed and discussed. Thirdly, an improved size-reduction design is proposed. Both designs are fabricated and measured, and the measurements agree with the predictions. A conclusion is drawn in the end.

## II. ANALYSIS OF THE CBCPW BALANCED BPF

A 2-order uniform-impedance resonator (UIR) with separated electric and magnetic coupling which is constructed by two $\lambda_g/4$ short-circuited resonators with width of $w_1$ is presented, as Figure 1(a) shows, and the equivalent transmission line circuit is shown in Figure 1(b). Where $\lambda_g$ is the guided wavelength, $\theta_c$ is the electric length corresponding to physical length of $(l_5 - w_2)/2 + l_3 + l_4$, $\theta_a$ and $\theta_b$ are the electric lengths corresponding to physical lengths of $l_1$ and $l_2$, respectively. $Z_a = Z_c$. Electric length can be expressed as $\theta = \omega_0 \cdot l \sqrt{\varepsilon_{re}}/c$, where $\omega_0$ is the resonant angular frequency, $l$ is the physical length, $\varepsilon_{re}$ is the effective permittivity, and $c$ is the velocity of light in free space.

As are labeled in Figure 1(a), the electric coupling is introduced by the gap of the parallel coupled lines with length of $l_2$, while the magnetic coupling is introduced by the grounding stub with width of $w_2$. The electric and the magnetic couplings are coexists but in different paths. Separated electric and magnetic coupling paths are essential for controllable transmission zero [12].

The ideal circuit of the proposed balanced bandpass filter by using the 2-order separated electric and magnetic coupling resonator is shown in Figure 2. The electrical coupling between resonators mainly occurs at the gap of the parallel coupled lines which are denoted by $Z_{ob}$, $Z_{eb}$ and $\theta_b$, while the magnetic coupling mainly concentrating around the
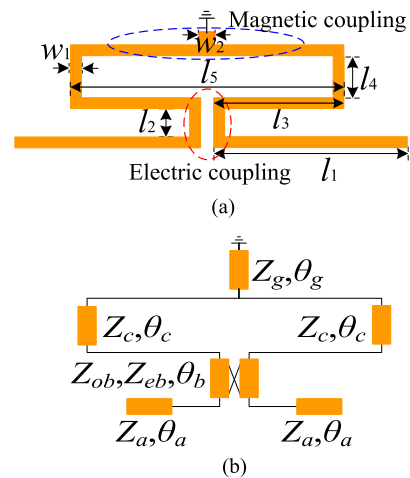


FIGURE 1. 2-order uniform resonator with SEMC. (a) Resonator structure. (b) Equivalent transmission line circuit.
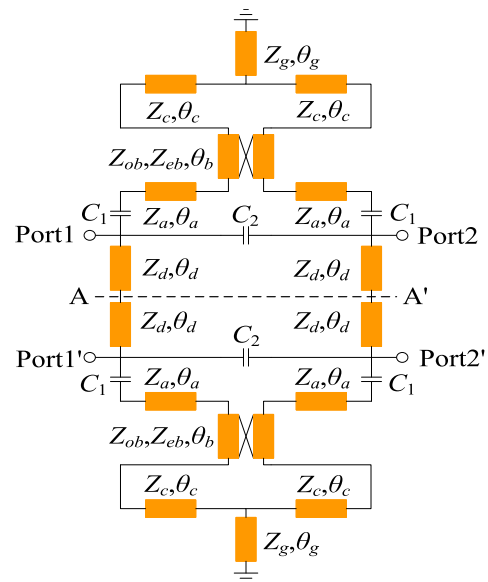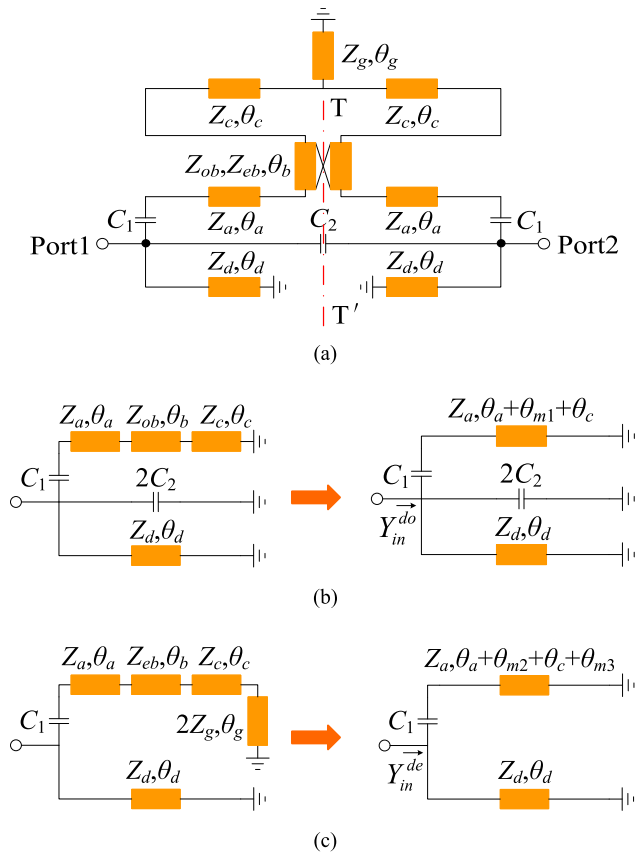


FIGURE 2. Equivalent transmission line circuit of the proposed balanced BPF.

grounding stub which is denoted by $Z_g$ and $\theta_g$. $C_1$ represents the coupling capacitance between the resonator and the feeder, while $C_2$ represents the coupling capacitance between the source and the load. A-A' is the symmetrical plane of the ideal circuit. $Z_d$ and $\theta_d$ represent a stub with guided wavelength of $\lambda_g/4$, and the filter common mode can be suppressed when the stub is open-circuited at the symmetrical plane.

### A. DIFFERENTIAL MODE ANALYSIS

The differential mode equivalent circuit can be obtained when A-A' is short-circuited, as is shown in Figure 3(a). The odd mode and the even mode equivalent circuits of the differential mode circuit can be obtained by using an electric wall and a magnetic wall on T-T', respectively. The odd

mode and the even mode equivalent circuits are exhibited in Figure 3(b) and (c), respectively.



FIGURE 3. Differential mode equivalent circuit and its odd/even mode circuits. (a) Differential mode equivalent circuit. (b) Odd mode circuit in DM. (c) Even mode circuit in DM.

For the odd mode equivalent circuit, transmission lines $(Z_a, \theta_a)$, $(Z_{ob}, \theta_b)$ and $(Z_c, \theta_c)$ can be equivalent as $(Z_a, \theta_a + \theta_{m1} + \theta_c)$. Where

$$Z_a = Z_c \tag{1a}$$

$$\theta_{m1} = \tan^{-1}(\frac{Z_{ob}}{Z_a} \tan \theta_b) \tag{1b}$$

The input admittance for each part shown in Figure 3(b) can be expressed as

$$Y_{o1} = -j\frac{1}{Z_a \tan (\theta_a + \theta_{m1} + \theta_c)} \tag{2a}$$

$$Y_{o2} = j\omega_{od}C_1 \tag{2b}$$

$$Y_{o3} = j2\omega_{od}C_2 \tag{2c}$$

$$Y_{o4} = -j\frac{1}{Z_d \tan \theta_d} \tag{2d}$$

The total input admittance of the odd mode equivalent circuit can be obtained as

$$Y_{in}^{do} = \frac{Y_{o1} \cdot Y_{o2}}{Y_{o1} + Y_{o2}} + Y_{o3} + Y_{o4} \tag{3}$$

While for the even-mode equivalent circuit as is illustrated in Figure 3(c), transmission lines $(Z_a, \theta_a)$, $(Z_{eb}, \theta_b)$, $(Z_c, \theta_c)$

and $(2Z_g, \theta_g)$ can be equivalent to $(Z_a, \theta_a + \theta_{m2} + \theta_c + \theta_{m3})$. Where

$$\theta_{m2} = \tan^{-1}(\frac{Z_{eb}}{Z_a} \tan \theta_b) \tag{4a}$$

$$\theta_{m3} = \tan^{-1}(\frac{2Z_g}{Z_a} \tan \theta_g) \tag{4b}$$

The input admittance for each part can be formulated as

$$Y_{e1} = -j\frac{1}{Z_a \tan (\theta_a + \theta_{m2} + \theta_c + \theta_{m3})} \tag{5a}$$

$$Y_{e2} = j\omega_{ev}C_1 \tag{5b}$$

$$Y_{e3} = -j\frac{1}{Z_d \tan \theta_d} \tag{5c}$$

The total input admittance of the even mode equivalent circuit can be expressed as

$$Y_{in}^{de} = \frac{Y_{e1} \cdot Y_{e2}}{Y_{e1} + Y_{e2}} + Y_{e3} \tag{6}$$

Here $C_2$ can be omitted because it is small enough and can not exert an influence on the resonant frequency. When $\theta_d = 90°$, $Y_{in}^{do} = Y_{in}^{de} = 0$, Resonant conditions of the odd mode and the even mode in DM can be expressed respectively as

$$1 - \frac{Z_{ob}}{Z_a} \tan (\theta_a + \theta_c) \cdot \tan (\theta_b) = 0 \tag{7}$$

$$1 - \frac{2Z_{eb}Z_g}{(Z_a)^2} \tan (\theta_b + \theta_g) - \frac{Z_{eb}}{Z_a} \tan (\theta_a + \theta_c) \tan \theta_b$$
$$+ \frac{2Z_g}{Z_a} \tan (\theta_a + \theta_c) \tan \theta_g = 0 \tag{8}$$

### B. COMMON MODE ANALYSIS

When the common mode signals are excited, the CM equivalent circuit can be achieved when the symmetrical plane A-A' is regarded as a perfect magnetic wall, as shown in Figure 4(a). In a similar analysis method as the differential mode circuit, the odd mode and the even mode equivalent circuits in CM can be obtained, as are illustrated in Figure 4(b) and (c), respectively. It can be calculated that when $\theta_d = 90°$, both the odd mode and the even mode input admittances can be obtained as $Y_{in}^{co} = Y_{in}^{ce} = \infty$, so, when the common mode signals have been excited, the CM suppression of the balanced BPF can be achieved because of the rejection band characteristic in the differential mode working frequency.
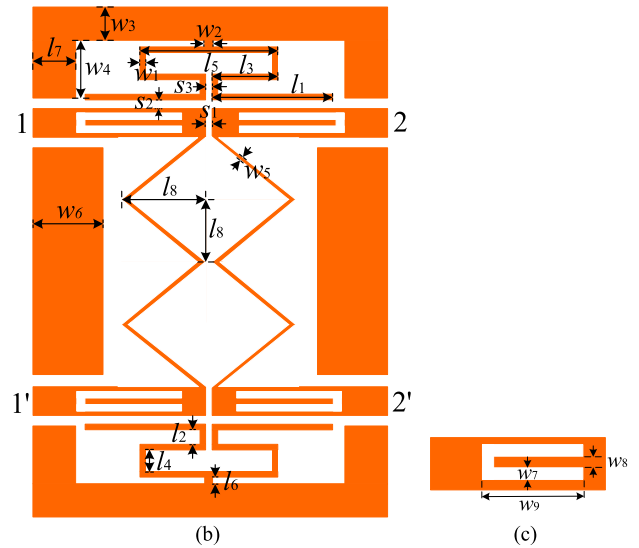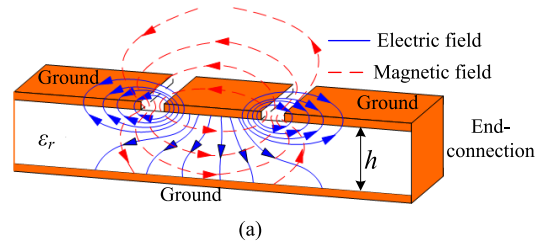
### C. BALANCED BANDPASS FILTER IMPLEMENTATION

The balanced bandpass filter is specified with center frequency of 2.32GHz, 3dB bandwidth of 11%, return loss of 25dB, and CM suppression of more than 27dB in the DM passband. The circuit is designed on a Teflon substrate with dielectric constant of 2.2 and a thickness of 0.8mm. Based on the above circuit analysis for the DM/CM, and full-wave modeled by HFSS, an interesting physical topology of the end-connected CBCPW balanced bandpass filter have been constructed, as shown in Figure 5. Where Figure 5(a) is the three dimensional topology of the end-connected CBCPW and its electromagnetic field, Figure 5(b) is the top view of
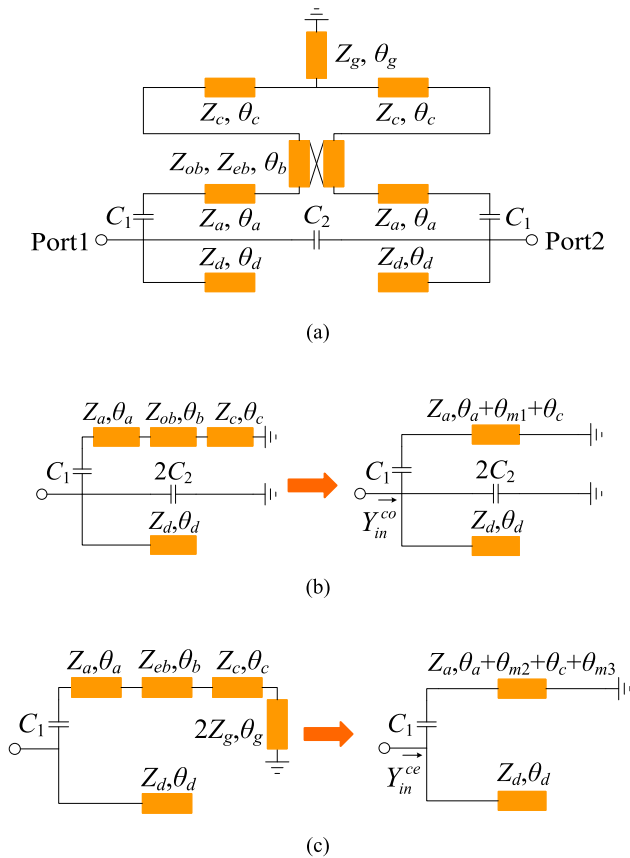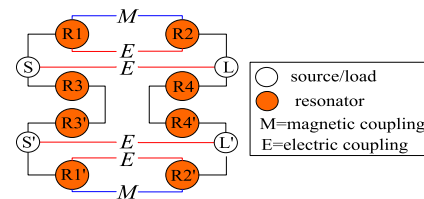
FIGURE 4. Common mode equivalent circuit and its odd/even mode circuits. (a) Common mode equivalent circuit. (b) Odd mode equivalent circuit in CM. (c) Even mode equivalent circuit in CM.



FIGURE 5. Physical topology of the proposed balanced BPF. (a) End-connected CBCPW and its electromagnetic field. (b) Top view of the end-connected CBCPW balanced BPF. (c) Defected feeding line.



FIGURE 6. Coupling structure of the end-connected CBCPW balanced BPF.

the proposed balanced BPF, and Figure 5(c) is the defected feeding line which is used to improve the circuit performance. To the best knowledge of the authors, it is the first time that the balanced BPF has been designed by the end-connected CBCPW structure. The circuit dimensions have been obtained as $l_1 = 11.0$, $l_2 = 1.0$, $l_3 = 6.0$, $l_4 = 1.5$, $l_5 = 12.6$, $l_6 = 0.4$, $l_7 = 6.8$, $l_8 = 8.5$, $s_1 = 0.2$, $s_2 = 0.2$, $s_3 = 0.6$, $w_1 = 0.7$, $w_2 = 0.5$, $w_3 = 3.0$, $w_4 = 4.46$, $w_5 = 0.5$, $w_6 = 9.0$, $w_7 = 0.8$, $w_8 = 0.2$ and $w_9 = 14.5$, unit: mm. The characteristic impedances of the equivalent circuit can be achieved as $Z_a = Z_c = 140.3$ohm, $Z_{ob} = 98.2$ohm, $Z_{eb} = 162.7$ohm, $Z_g = 74.5$ohm. Coupling structure of the proposed balanced BPF is plotted in Figure 6. It can be seen clearly that the electric coupling and the magnetic coupling coexist but they are in different paths.

For the certain dimensions, the odd/even mode resonant frequencies of the DM can be calculated as 2.38 GHz ($f_{od}$) and 2.29 GHz ($f_{ev}$), respectively, by formulas (7) and (8). The calculation approaches to the simulated odd mode resonant frequency of 2.32GHz, and the even mode resonant frequency of 2.25GHz, which demonstrates the equivalent transmission line circuit model of the end-connected CBCPW balanced BPF.

Simulated electric and magnetic field distributions of the proposed balanced bandpass filter at center frequency of 2.32GHz are illustrated in Figure 7. It can be seen that the electric field is concentrated around the electric coupling gap $s_3$, while the magnetic field is around the grounding stub $w_2$. Which demonstrates the electric/magnetic coupling paths as shown in Figure 1(a) and Figure 6.

Comparison of the simulated current distributions for the CBCPW balanced bandpass filter with and without end-connection are shown in Figure 8. It can be seen that for the same circuit dimensions and center frequency, the electromagnetic field for the end-connected CBCPW structure is stronger than that without end-connection, which indicates that the end-connected CBCPW structure has stronger electromagnetic (EM) coupling, and the enhanced EM coupling
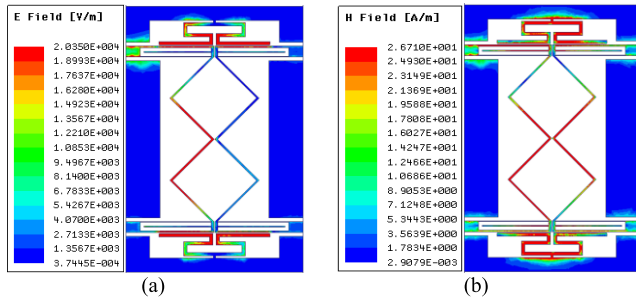
**FIGURE 7.** Simulated electric/magnetic field distributions at 2.35GHz. (a) Electric field distribution. (b) Magnetic field distribution.
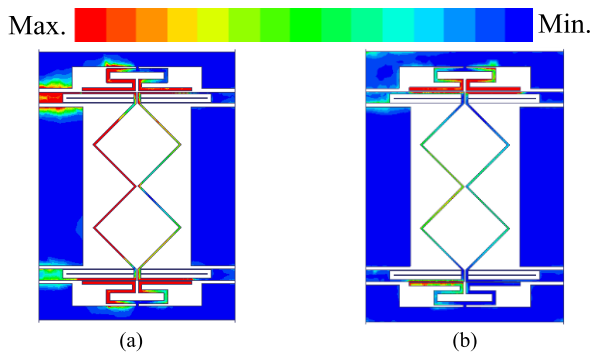


**FIGURE 8.** Comparison of the simulated current distributions with and without end-connection. (a) CBCPW balanced BPF with end-connection. (b) CBCPW balanced BPF without end-connection.

is due to the end-connection which further reduces the electromagnetic wave leakage.

For the certain circuit dimensions, simulated DM/CM frequency responses comparison with and without feeding defection are illustrated in Figure 9 (a) and (b), respectively. It can be seen clearly that the proposed filter has a passband insertion loss of 1.0dB at the center frequency, which lowers more than 1.4dB compared with the structure without feeding defection, while has a fractional bandwidth enhancement of about 61%. It also shows in Figure 9(b) that with feeding defection, there is a wider and higher common mode suppression in the DM band compared with the structure without feeding defection. The improvement of the insertion loss and bandwidth are due to the feeding defection which enhances the electromagnetic coupling.

## III. ANAALYSIS OF TRANSMISSION ZEROS AND BANDWIDTH

The electric/magnetic coupling concentrates between resonators R1-R2, and resonators R1'-R2', as is shown in Figure 6. Transmission zero is attributed to the electric/magnetic coupling. The electric and magnetic coupling coefficients can be denoted as $k_e$ and $k_m$, respectively. Where $k_e = C_m/C$, $k_m = L_m/L$, $L$ and $C$ are self-coupling inductors and capacitors of resonators, respectively, while $L_m$ and $C_m$ are coupling inductance and coupling capacitance, respectively. $L_m$ and $C_m$ can be obtained by electromagnetic
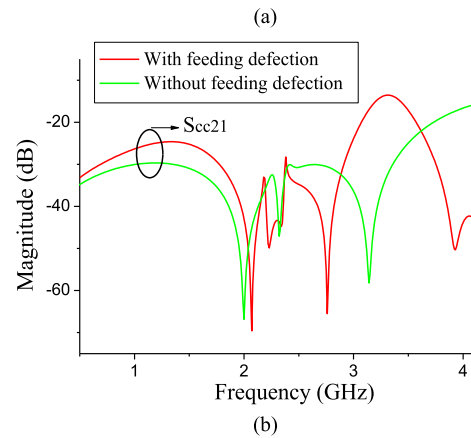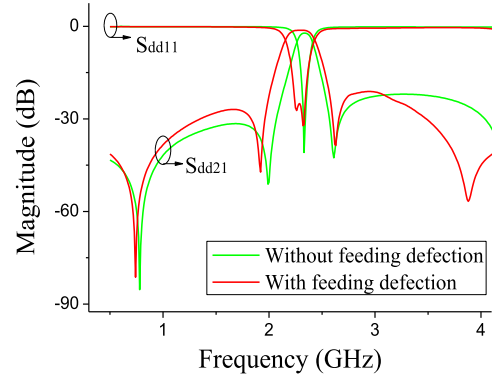


**FIGURE 9.** Comparison of the DM/CM frequency responses with and without feeding defection. The circuit dimensions without feeding defection are $l_1$=11.0, $l_2$=1.0, $l_3$=6.0, $l_4$=1.5, $l_5$=12.6, $l_6$=0.4, $l_7$=3.9, $l_8$=8.5, $s_1$=0.4, $s_2$=0.3, $w_1$=0.3, $w_2$=0.5, $w_3$=3.0, $w_4$=3.7, $w_5$=0.35, and $w_6$=6.0, unit: mm. (a) DM frequency responses comparison. (b) CM frequency responses comparison.

coupling theory in [13] by solving the formulas as follows.

$$f_e = \frac{1}{2\pi\sqrt{(L-L_m)(C-C_m)}} \tag{9}$$

$$f_m = \frac{1}{2\pi\sqrt{(L+L_m)(C+C_m)}} \tag{10}$$

where $f_e$ and $f_m$ are the resonances of the odd mode and the even mode for the resonator as shown in Figure 1(a), respectively, which can be obtained by electromagnetic simulation. The simulated frequency responses on TZs versus magnetic/electric coupling variations are plotted in Figure 10(a), and (b), respectively, where $f_{TZi}$ is the frequency of the *i*-th transmission zero.

TZs variation versus grounding stub width $w_2$ is shown in Figure 10(a). It can be seen that when $w_2$ increases from 0.3mm to 0.7mm, namely, the magnetic coupling strength is lowered, $f_{TZ1}$ increases to a higher frequency to be closer to the center frequency of the DM response, while $f_{TZ2}$ nearly keeps unchanged. It is also noted in the research that when $w_2 = 0$, $f_{tz1}$ can not be produced. So it can be concluded that $f_{TZ1}$ is controlled by the magnetic-dominant coupling (M-coupling). It is seen from Figure 10(b) that when the electric coupling gap $s_3$ increases from 0.3mm to 0.6mm, namely,
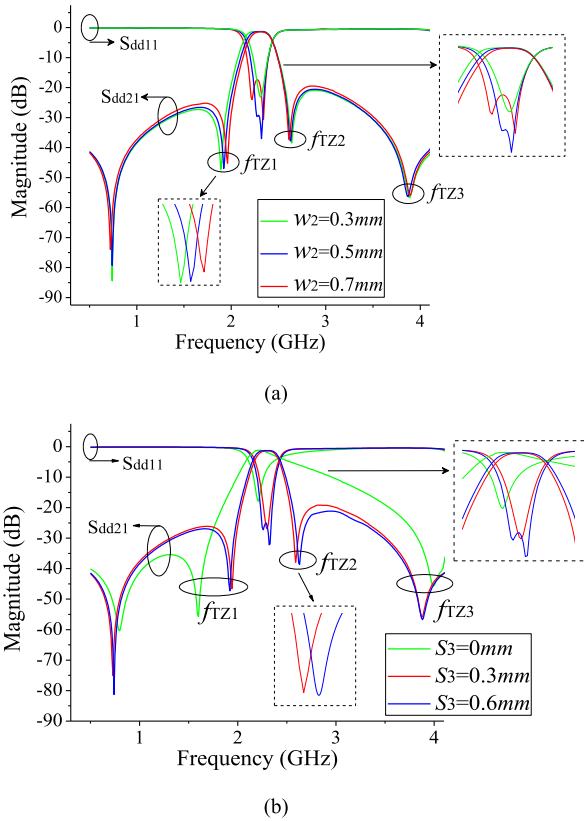
(a)



(b)

**FIGURE 10.** TZs versus electric/magnetic coupling variations. (a) TZs variation versus the magnetic coupling determinant $w_2$. (b) TZs variation versus electric coupling gap $s_3$.

the electric coupling strength is lowered, $f_{TZ2}$ increases to a higher frequency which is further away from the center frequency of the DM response, while $f_{TZ1}$ nearly has no change. It is also noticed that when $s_3 = 0$, $f_{TZ2}$ can not be obtained. So it can be concluded that $f_{TZ2}$ is controlled by the electric-dominant coupling (E-coupling). So, $f_{TZ1}$ and $f_{TZ2}$ can be adjusted independently by the magnetic-dominant coupling and the electric-dominant coupling, respectively.

Extracted electric/magnetic coupling coefficients versus coupling gap $s_3$ and grounding stub width $w_2$ are listed in Table 1 and Table 2, respectively. It is seen that the electric/magnetic coupling coefficients are appropriate with the electric/magnetic coupling strength. $k_e$ decreases with coupling gap $s_3$ increasing, while $k_m$ decreases with $w_2$ increasing, both bring reduced electric/magnetic couplings.

**TABLE 1.** Electric coupling coefficient versus coupling gap $s_3$.

| $s_3$ (mm) | $k_e$ | $C_m$ (pF) | $C$ (pF) |
|---|---|---|---|
| 0.4 | 0.147 | 0.056 | 0.38 |
| 0.6 | 0.118 | 0.045 | 0.38 |

For the magnetic-dominant coupling controlled TZ, the TZ frequency location can be formulated as

$$f_{TZm} = f_0\sqrt{k_e/k_m} \qquad (11)$$

**TABLE 2.** Magnetic coupling coefficient versus $w_2$.

| $w_2$ (mm) | $k_m$ | $L_m$ (nH) | $L$ (nH) |
|---|---|---|---|
| 0.1 | 0.198 | 2.41 | 12.2 |
| 0.3 | 0.182 | 2.22 | 12.2 |
| 0.6 | 0.157 | 1.92 | 12.2 |

While for the electric-dominant coupling controlled TZ, the TZ frequency location can be formulated as [14]

$$f_{TZe} = f_0\sqrt{k_m/k_e} \qquad (12)$$

where $f_0$ is the filter center frequency, $k_m$ and $k_e$ are absolute value. It can be calculated that for $k_e = 0.118$, and $k_m = 0.157$, the frequency location of the magnetic-dominant coupling $f_{TZ1} = f_{TZm} = 2.03$GHz, while the TZ location of the electric-dominant coupling $f_{TZ2} = f_{TZe} = 2.71$GHz, which approach to the simulated results of 1.93/2.63GHz, respectively, as shown in Fig. 9(a).

It also can be seen from Figure 10(a) and (b) that the variations of electric/magnetic couplings make a corresponding variation of filter bandwidth. Figure 10(a) shows that when $w_2$ increases from 0.3mm to 0.7mm, it is to say that for the magnetic coupling decreasing, the fractional bandwidth of the balanced BPF decreased from 11.44% to 8.26%. It is seen in Figure 10(b) that when $s_3$ increases from 0.3mm to 0.6mm, namely the electric coupling decreases, the fractional bandwidth of the balanced BPF increased from 8.68% to 10.65%, as are demonstrated by the solid lies in red and blue. As the electric/magnetic couplings and the total coupling have been numerically formulated by $k_e$, $k_m$, and $k = k_m - k_e$, respectively [13], the filter bandwidth can also be adjusted by either $k_e$ or $k_m$, or by $k$ because which is determined by both $k_e$ and $k_m$. The filter bandwidth adjustment rules based on coupling coefficients are similar to that of $w_2/s_3$ variations, as have been described.
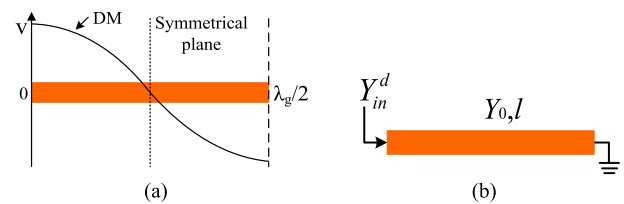


(a)                                    (b)

**FIGURE 11.** The equivalent circuit model of the half-wavelength resonator in differential-mode. (a) The voltage distribution of the half-wavelength resonator when the differential mode signal is excited. (b) Short-circuited quarter-wavelength resonator.

The meandered line resonator which connects with port 1 and 1' as shown in Figure 5(c) is a half-wavelength resonator. When the differential mode signal is excited, the voltage of the resonator at the symmetrical plane is zero, as shown in Figure 11(a), which can be regarded as a short-circuited quarter-wavelength resonator, as is shown in Figure 11(b). The differential-mode quarter-wavelength resonator has been denoted by $\theta_d$ and $Z_d$ in Figure 3(a).

According to the transmission line theory, the input admittance $Y_{in}^d$ of the short-circuited quarter-wavelength resonator can be expressed as

$$Y_{in}^d = -j\frac{Y_0}{\tan\beta l} \qquad (13)$$

When $\theta_d = 90°$, resonant condition of $Y_{in}^d = 0$ can be achieved, while when $Y_{in}^d = \infty$ ($S_{21} = 0$), $f_{TZ3}$ can be generated, and its frequency location can be formulated from (13) as

$$f_{tz3} = \frac{c}{2l\sqrt{\varepsilon_{re}}} \qquad (14)$$

When $l = l_8 = 8.5$mm, $f_{TZ3}$ can be obtained by equation (14) as 4.66 GHz, which approaches to the simulated results without feeding defection of 4.23GHz. In this research, it is noted that feeding defections enhance filter bandwidth, simultaneously reduce the frequency location of $f_{TZ3}$, for example 3.92GHz in this design, as shown in Figure 10(a). It indicates that $f_{TZ3}$ can be adjusted not only by the circuit physical length $l_8$, but also by the feeding defection.

## IV. COMMON MODE SUPPRESSION

CM suppression of the proposed end-connected CBCPW balanced BPF is dominantly controlled by the meandered lines connecting with the source/load. When the common-mode signal is excited, the voltage of the half-wavelength resonator at the symmetrical plane has the maximum value, while the current can be seen as zero, as shown in Figure 12(a), so which can be regarded as a open-circuited quarter-wavelength resonator, as is shown in Figure 12(b). The open-circuited quarter-wavelength resonator is applied to realize the common mode suppression because which has stopband characteristic at the center frequency.
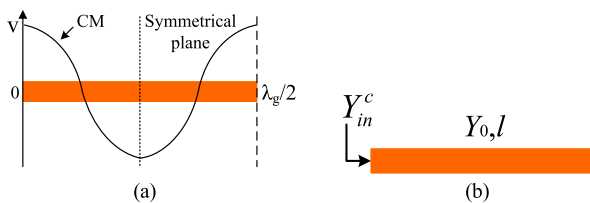


**FIGURE 12.** The equivalent circuit model of the half-wavelength resonator in common mode. (a) The voltage distribution of the half-wavelength resonator when the common mode signal is excited. (b) Open-circuited quarter-wavelength resonator.

Simulated DM and CM frequency responses versus parameters $l_8$ and $w_5$ are illustrated in Figure 13 and Figure 14, respectively. It can be seen from Figure 13(a) and (b) that the variation of $l_8$ has little effect on the basic DM frequency response, but obvious effect on the CM suppression. When the resonator length approaches to quarter-wavelength, the best CM suppression can be achieved. Figure 14(a) and (b) show that the variation of $w_5$ nearly has no effect on the DM response, but obvious effect on the CM suppression.
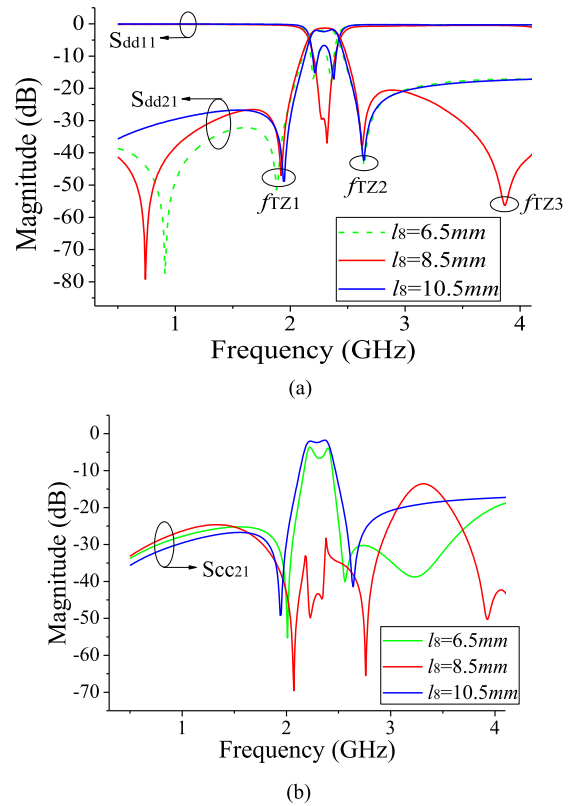


**FIGURE 13.** DM and CM frequency responses versus parameter $l_8$. (a) DM response variation versus $l_8$. (b) CM response variation versus $l_8$.

So it is concluded that the DM and the CM responses can be controlled and adjusted individually, which improves the design flexibility importantly.

For the certain circuit dimensions as have been shown in part II, the common mode rejection ratio (CMRR) can be obtained by CMRR$=-20\log(|S_{dd21}|/|S_{cc21}|)$ [15] , the calculation result is plotted in Figure 15. It is seen that the in-band common mode suppression is from 27.3dB to 48.7dB, while the CMRR at center frequency of 2.32GHz is about 40dB, which is higher than some related reports as in [6], [11], [16], and [17].

## V. FABRICATION AND MEASUREMENT

The proposed end-connected CBCPW balanced bandpass filter has been fabricated and measured, as is shown in Figure 16. Where Figure 16(a) is the fabricated hardware, Figure 16(b) is the differential mode responses, and Figure 16(c) is the common mode responses. The fabrication is measured by Agilent E5071C vector network analyzer.

It is seen from the measurement in Figure 16(b) that the balanced BPF centers at 2.35GHz with a 3dB fractional bandwidth (FBW) of 10.5%, a passband insertion loss of 1.3dB at center frequency, and a return loss of more than 21dB, all these agree with the predictions except for a slight frequency shift. The measured four TZs are located at 0.79/1.97/2.68/4.11GHz, which approach to the
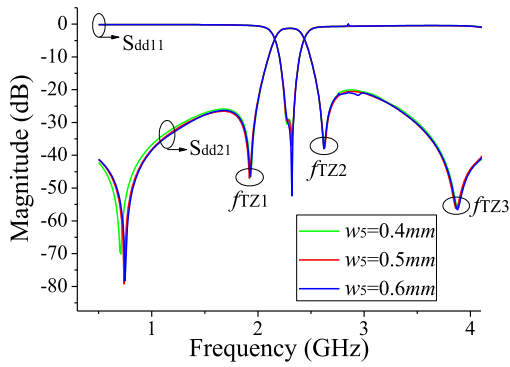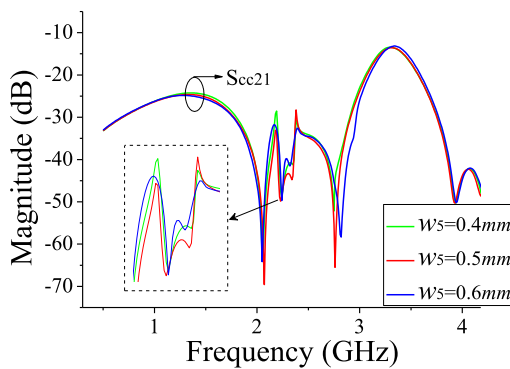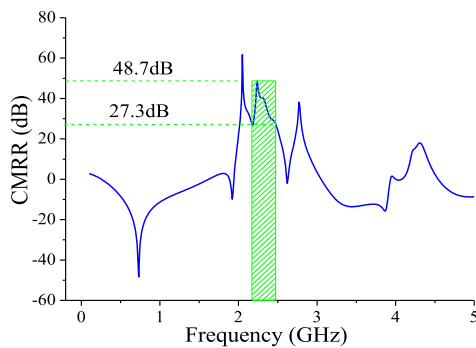
**FIGURE 14.** DM and CM frequency responses versus parameter $w_5$. (a) DM response variation versus $w_5$. (b) CM response variation versus $w_5$.



**FIGURE 15.** Simulated CMRR variation in 3dB DM band.

simulated zero points of 0.74/1.91/2.62/3.92GHz. The discrepancy between the simulation and the measurement is due to the material/fabrication uncertainty and the measurement system errors. The measured out-of-band rejection is over 24.8dB from 0.03GHz to 4.0 GHz. From the measured CM response shown in Figure 16(c), it is seen that the CM suppression in DM passband is more than 42dB, while the CM suppression out-of DM passband is more than 13.6dB from 0.03-5.0GHz. The measured CMRR at center frequency is about 30.19dB. The whole circuit size of the proposed balanced bandpass filter is $0.38\lambda_g \times 0.58\lambda_g$, which has a circuit size reduction of 14.61%, 74.80% and 83.12% compared
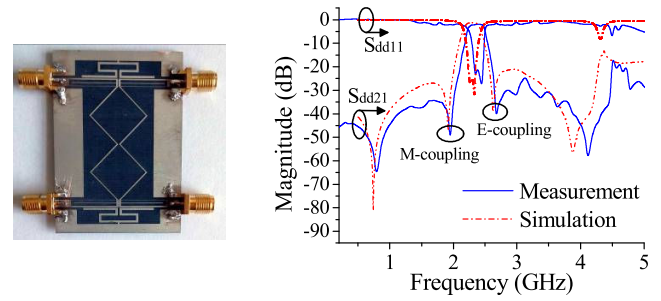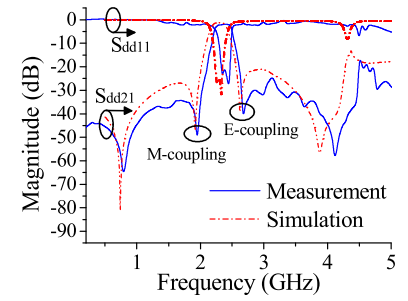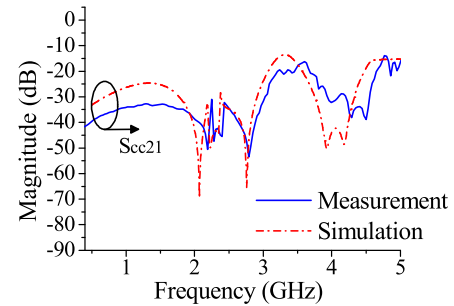


**FIGURE 16.** Fabrication and comparison of the simulation/measurement for the proposed end-connected CBCPW balanced BPF. (a) Fabricated hardware. (b) Differential mode responses. (c) Common mode responses.

with [5]–[7], respectively. Where $\lambda_g$ is the guided wavelength at 2.35GHz.
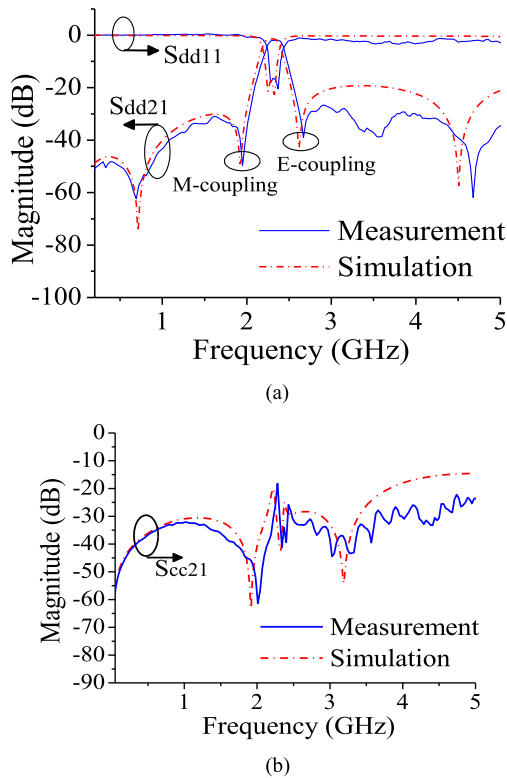
## VI. MODIFIED BALANCED BANDPASS FILTER
A modified balanced bandpass filter with end-connected CBCPW is also proposed with a center frequency of 2.3GHz, FBW of 7.8%, passband insertion loss of 1.1dB, and a return loss of 18dB, as is shown in Figure 17(a). Where the meandered lines that connect with the source/load have been stair folded in order to reduce the circuit size. $l_9 = 0.6$mm, $l_{10} = 3.3$mm, $w_1 = 0.5$mm, $w_7 = 0.7$mm, $w_8 = 3.9$mm. The circuit size of the modified balanced BPF is $0.34\lambda_g \times 0.42\lambda_g$, which has a size reduction of 35.2% compared with the proposed filter structure shown in Figure 5(c).

The modified balanced BPF has also been fabricated and measured. The fabrication photograph is illustrated in Figure 17(b), while the measured/simulated frequency responses for the DM and CM are plotted in Figure 18(a) and (b), respectively. For the DM response as shown in Figure 18(a), the measurement shows that the modified balanced bandpass filter has a center frequency of 2.32GHz, a FBW of 6.9%, an insertion loss of 1.4dB, and a return loss of more than 16dB. It can be seen that the measurement approaches to the prediction. Four transmission zeros which locate at 0.69/1.94/2.64/4.69GHz have been realized. Moreover, the out-of-band rejection is over 25.8dB from 0.03GHz to 5.0GHz. For the common mode response as shown in Figure 18(b), it is seen that the measured CM suppression at center frequency is more than 35dB, while
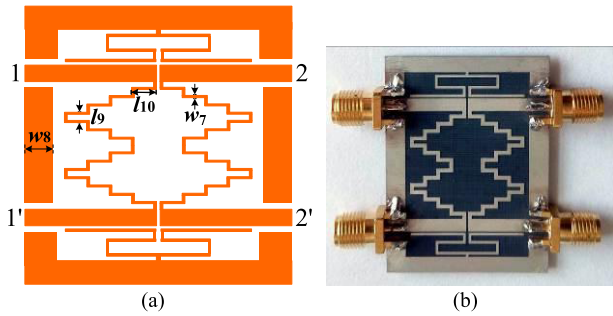
**FIGURE 17.** Topology of the modified end-connected CBCPW balanced BPF and the fabricated hardware. (a) The proposed BPF topology. (b) Fabrication.



**FIGURE 18.** Comparison of the simulation/measurement for the modified balanced bandpass filter. (a) Differential mode responses. (b) Common mode responses.

the measured CM suppression from 0.03GHz to 5.0GHz is more than 18.4dB. The measurement approaches to the simulation. Measured CMRR at center frequency can be obtained as 27.96dB.

Table 3 exhibits the measurement comparison of the proposed designs with some related reports. It can be seen that the proposed end-connected CBCPW balanced BPFs have more transmission zeros than [5]–[7], [10], and [17], while keep the other performance such as IL and CM suppression not differ much, even better than the relative reports. The proposed works also have advantages of more compact circuit sizes compared with the related reports in [5]–[7], and controllable/adjustable TZs and bandwidth compared

**TABLE 3.** Comparison of measurement with some related works.

| References | CT/CF (GHz) | IL/RL (dB) | TZs | In-band CM rejection (dB) | Size ($\lambda g \times \lambda g$) |
|---|---|---|---|---|---|
| [5] | MS/2.42 | 0.8/10 | 0 | >35 | 0.2×1.29 |
| [6]Fig.11(a) | MS/6.85 | 0.8/12.5 | 2 | >13.5 | 0.73×1.2 |
| [7]Fig.8 (a) | MS/3.1 | 1.65/15 | 2 | >40 | 1.07×1.22 |
| [10]Fig.5 | MS/2.45 | 1.28/40 | 0 | >40 | 0.195×0.246 |
| [17]Fig.2 | MS/1.57 | 0.95/27.5 | 0 | >25 | 0.182×0.24 |
| This work 1 | CBCPW /2.35 | 1.3/21 | 4 | >42 | 0.38×0.58 |
| This work 2 | CBCPW /2.32 | 1.4/16 | 4 | >35 | 0.34×0.42 |

CT-circuit type, CF-center frequency, MS-microstrip, IL-insertion loss, RL-return loss.

with [5]–[7], [10], and [17]. The modified balanced BPF has similar performance with the first proposed one but has an obviously reduced circuit size. The circuit sizes in this work include the source and the load.
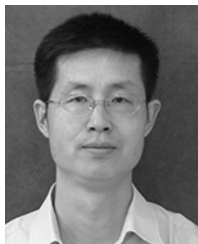
## VII. CONCLUSION

In this paper, new end-connected CBCPW balanced bandpass filters with multiple adjustable transmission zeros, good common mode suppression, wide out-of-band suppression and compact circuit sizes have been developed. Transmission zeros are attributed to the electric/magnetic couplings and the quarter-wavelength short-circuited stubs, and three of these transmission zeros can be controlled/adjusted flexibly. Simultaneously, the DM and the CM parts can be individually designed because they have much less effect on each other, which greatly improves the design flexibility. The proposed works also have better electromagnetic shielding because of the end-connection structure and the conductor strip/ground co-plane.

## REFERENCES

[1] T. B. Lim and L. Zhu, "A differential-mode wideband bandpass filter on microstrip line for UWB application," *IEEE Microw. Wireless Compon. Lett.*, vol. 19, no. 10, pp. 632–634, Oct. 2009.

[2] T. B. Lim and L. Zhu, "Differential-mode ultra-wideband bandpass filter on microstrip line," *Electron. Lett.*, vol. 45, no. 22, pp. 1124–1125, Oct. 2009.

[3] T. B. Lim and L. Zhu, "Highly selective differential-mode wideband bandpass filter for UWB application," *IEEE Microw. Wireless Compon. Lett.*, vol. 21, no. 3, pp. 133–135, Mar. 2011.

[4] Z.-A. Ouyang and Q.-X. Chu, "An improved wideband balanced filter using internal cross-coupling and 3/4λ stepped-impedance resonator," *IEEE Microw. Wireless Compon. Lett.*, vol. 26, no. 3, pp. 156–158, Mar. 2016.

[5] H. Wang, K.-W. Tam, S.-K. Ho, W. Kang, and W. Wu, "Short-ended self-coupled ring resonator and its application for balanced filter design," *IEEE Microw. Wireless Compon. Lett.*, vol. 24, no. 5, pp. 312–314, May 2014.

[6] W. Feng and W. Che, "Novel wideband differential bandpass filters based on T-shaped structure," *IEEE Trans. Microw. Theory Techn.*, vol. 60, no. 6, pp. 1560–1568, Jun. 2012.

[7] W. Feng, W. Che, and Q. Xue, "Balanced filters with wideband common mode suppression using dual-mode ring resonators," *IEEE Trans. Circuits Syst. I, Reg. Papers*, vol. 62, no. 6, pp. 1499–1507, Jun. 2015.

[8] X. Guo, L. Zhu, K.-W. Tam, and W. Wu, "Wideband differential bandpass filters on multimode slotline resonator with intrinsic common-mode rejection," *IEEE Trans. Microw. Theory Techn.*, vol. 63, no. 5, pp. 1587–1594, May 2015.

[9] T. Yan, D. Lu, J. Wang, and X.-H. Tang, "High-selectivity balanced bandpass filter with mixed electric and magnetic coupling," *IEEE Microw. Wireless Compon. Lett.*, vol. 26, no. 6, pp. 398–400, Jun. 2016.

[10] A. Fernández-Prieto, A. Lujambio, J. Martel, F. Medina, F. Mesa, and R. R. Boix, "Simple and compact balanced bandpass filters based on magnetically coupled resonators," *IEEE Trans. Microw. Theory Techn.*, vol. 63, no. 6, pp. 1843–1853, Jun. 2015.

[11] Q.-X. Chu and L.-L. Qiu, "Wideband balanced filters with high selectivity and common-mode suppression," *IEEE Trans. Microw. Theory Techn.*, vol. 63, no. 10, pp. 3462–3468, Oct. 2015.

[12] K. Ma, J.-G. Ma, K. S. Yeo, and A. V. Do, "A compact size coupling controllable filter with separate electric and magnetic coupling paths," *IEEE Trans. Microw. Theory Techn.*, vol. 54, no. 3, pp. 1113–1119, Mar. 2006.

[13] J.-S. Hong and M. J. Lancaster, *Microstrip Filters for RF/Microwave Applications*. New York, NY, USA: Wiley, 2001.

[14] H. Wang and Q. X. Chu, "An EM-coupled triangular open-loop filter with transmission zeros very close to passband," *IEEE Microw. Wireless Compon. Lett.*, vol. 19, no. 2, pp. 71–73, Feb. 2009.

[15] C.-H. Wu, C.-H. Wang, and C. H. Chen, "Novel balanced coupled-line bandpass filters with common-mode noise suppression," *IEEE Trans. Microw. Theory Techn.*, vol. 55, no. 2, pp. 287–295, Feb. 2007.

[16] X.-H. Wu, Q.-X. Chu, and L.-L. Qiu, "Differential wideband bandpass filter with high-selectivity and common-mode suppression," *IEEE Microw. Wireless Compon. Lett.*, vol. 23, no. 12, pp. 644–646, Dec. 2013.

[17] J. Shi and Q. Xue, "Balanced bandpass filters using center-loaded half-wavelength resonators," *IEEE Trans. Microw. Theory Techn.*, vol. 58, no. 4, pp. 970–977, Apr. 2010.

**XING QI** was born in Hebei, China. He received the B.S. degree in electronic science and technology from Yanshan University, China, in 2015. He is currently pursuing the M.S. degree with Xidian University, China. His research interest includes microwave-balanced filter design.

**HUI-XIA WANG** was born in Shaanxi, China. She received the B.S. degree in measurement and control technology and instrumentation from the Xi'an University of Science and Technology, China, in 2017. She is currently pursuing the M.S. degree with Xidian University, China. Her research interests include microwave filter/diplexer and multi-layer circuit design.

**JIAN-GUO MA** received the B.Sc. and M.Sc. degrees from Lanzhou University, China, in 1982 and 1988, respectively, and the Ph.D. degree in engineering from Duisburg University, Germany, in 1996. He was a Postdoctoral Fellow with the Technical University of Nova Scotia, Halifax, NS, Canada, from 1996 to 1997. He was a Faculty Member with Nanyang Technological University, Singapore, from 1997 to 2005, where he was also the Founding Director of the Center for Integrated Circuits and Systems. From 2005 to 2009, he was with the University of Electronic Science and Technology of China, China, and then, he joined Tianjin University, China. He is currently a Professor with the Guangdong University of Technology. He was a recipient of the prestigious Changjiang (Yangtze) Chair Professorship Award by the Ministry of Education of China in 2008; he was also the Distinguished Young Investigator that was awarded by the National Natural Science Foundation of China in 2008.

His research interests include RFICs and RF integrated systems for wireless, RF device characterization modeling, MMIC, RF/microwave circuits, and systems design.

**JIAN-KANG XIAO** received the B.S. degree in electronics and the M.S. degree in radio physics from Lanzhou University, China, in 1996 and 2004, respectively, and the Ph.D. degree from Shanghai University, China, in 2007. He was a Postdoctoral Research Fellow with the South China University of Technology, China, from 2007 to 2009. He joined Xidian University, China, in 2011. He was an Academic Visitor with Heriot-Watt University, U.K., from 2015 to 2016. His research interests include microwave passive components design and antennas. He was a Reviewer for many international journals, including the IEEE Transactions on Microwave Theory and Techniques, the IEEE MWCL, the *IEEE Microwave Magazine*, IET MAP, and *IET Electronics Letters*.

• • •